Jurnal Polimesin
Department of Mechanical Engineering
State Polytechnic of Lhokseumawe
http://e-jurnal.pnl.ac.id/polimesin

e-ISSN : 2549-1999 No. : 5 Month : October
p-ISSN : 1693-5462 Volume : 23 Year : 2025

Processing dates: received on 2025-07-28, reviewed on 2025-10-10, accepted on 2025-10-19 and online availability on 2025-10-31

Hybrid spot welding-epoxy bonding of AISI 1008 steel: Shear and nugget analysis

Paryanto Dwi Setyawan*, Irfan Hakiki, Sugiman, Salman, Sinarep, Andi Maulana

Department of Mechanical Engineering, Mataram University, Mataram, West Nusa Tenggara, 83125, Indonesia
*Corresponding author: paryanto.ds@unram.ac.id

Abstract

The growing demand for lightweight, high-performance structures in transportation and manufacturing has intensified research on hybrid weld-bonding as a joining method that synergizes the metallurgical strength of resistance spot welding (RSW) with the stress-damping capability of adhesives. However, the interaction between welding parameters, adhesive type, and adhesive thickness and their collective influence on nugget microstructure and joint integrity remains poorly understood. This study addresses these gaps through a systematic parametric investigation of hybrid spot weld–epoxy joints in AISI 1008 steel. Three commercial epoxy adhesives (Araldite 5 min, Araldite 90 min, and Devcon 90 min) were applied at thicknesses of 0.2, 0.6, and 1.0 mm under a fixed RSW schedule (50 A, 10 s), followed by a secondary factorial test varying welding current (50-80 A) and time (10-20 s) for Araldite 5 min at 0.6 mm. Mechanical performance was evaluated via lap shear testing, while fracture morphology and nugget chemistry were analyzed using optical microscopy, SEM, and EDX. Results revealed an optimal configuration at 60 A and 10 s with 0.6 mm Araldite 5 min adhesive, achieving the highest shear strength (~5.74 kN). Strength exhibited a non-monotonic dependence on adhesive thickness, indicating coupled thermo-mechanical effects of polymer decomposition and stress redistribution. Fractographic analysis showed transitions from interfacial to cohesive failure modes with increasing adhesive thickness, while excessive welding energy induced HAZ softening and porosity. The study advances mechanistic understanding by correlating adhesive curing kinetics and thermal degradation with nugget evolution and joint mechanics. These findings provide both scientific insight and practical guidance for optimizing hybrid joining parameters in thin-gauge steel structures.

Keywords:
Fracture modes, hybrid weld-bonding, joint macrostructure, nugget composition, shear characteristics.

1 Introduction

The relentless drive in transportation, aerospace, and structural engineering industries toward lighter, more durable, and cost-efficient assemblies has spurred intense interest in hybrid joining methods. Among these, hybrid spot welding–adhesive bonding (commonly called weld-bonding or weld-adhesive spot joining) offers an attractive synergy: the rapid energy input and metallurgical fusion of resistance spot welding, combined with the stress-redistribution, crack-bridging and fatigue resistance benefits of adhesive bonding. Traditional resistance spot welding (RSW) yields highly localized load-bearing capacity but suffers from concentrated stress, brittle failure modes, and limited adaptability under multi-axial loading. The adhesive layer, conversely, spreads shear and peel stresses, suppresses stress raisers, and helps improve fatigue and vibration performance [1], [2], [3]. In industrial practice (notably automotive OEMs and aerospace frames), hybrid weld-bonded joints have emerged as enabling techniques where both structural integrity and manufacturability are demanded. Guidance documents for advanced high-strength steel joining frequently propose combining adhesives with spot welding to mitigate distortion and stress concentration in body-in-white structures [4].

Over the past decade, numerous investigations have confirmed that hybrid weld-bonded configurations can outperform bare spot welds in fatigue life, corrosion resistance, energy absorption, and joint stiffness [5]-[11]. However, the majority of these studies restrict themselves to macroscopic metrics such as tensile-shear strength, fatigue crack growth rates, joint stiffness, and hardness distribution [3], [12]. While such results are important, they rarely probe how different adhesive formulations and thicknesses influence the thermochemical and microstructural evolution of the weld nugget and adjacent heat-affected zones. In particular, the phenomenon of adhesive decomposition during welding can alter instantaneous thermal cycles, local element diffusion, gas generation, and nugget porosity or inclusion formation, thereby affecting long-term reliability and failure modes-an area that has been only lightly addressed in past literature [6], [13].

Moreover, adhesive selection (e.g. curing kinetics, thermal stability) and adhesive thickness optimization remain heuristic in many prior works. Industrial practice often prescribes thin film adhesives (0.1-0.3 mm) to minimize interference with nugget formation, yet this may not be optimal under all welding energy regimes [3], [14], [15]. Studies such as Marques et al. [2] have explored how adhesives of different stiffness influence stress transfer in hybrid joints [2], and recent work showed that adhesives can even influence the fusion zone solidification dynamics and microstructure in weld bonding of steels [16]. However, systematic, parametric studies combining adhesive type, adhesive thickness, and spot welding parameters (current, time) in a single integrated experiment remain quite rare in peer-reviewed literature.

In particular for AISI 1008 (a low-carbon steel widely used as a baseline substrate in joining studies), few works have addressed hybrid spot weld–adhesive joints with a parametric sweep of adhesive types, thicknesses, and welding energy conditions. One somewhat comparable work describes “resistance spot weld assisted with adhesive bonding” on low-carbon steel (JIS G3141), using a single epoxy layer thickness and fixed spot weld power, focusing on strength and macro-etch observations [16]. But it lacks microstructural/EDX correlation and does not vary adhesive thickness or welding time systematically.

To fill these gaps, the present study carries out a systematic, factorial investigation of hybrid spot welding–adhesive bonding of AISI 1008 steel, in which adhesive type, adhesive thickness, spot welding current, and spot welding time are jointly varied. Specifically, the baseline matrix uses three epoxy adhesives (Araldite 5 min, Araldite 90 min, Devcon 90 min) and three thickness levels (0.2 mm, 0.6 mm, 1.0 mm), under a primary spot welding setting of 50 A, 10 s. In addition, a secondary sub-experiment varies between spot welding current over 50 A, 60 A, 70 A, 80 A and welding time over 10 s, 15 s, 20 s, using the Araldite 5 min adhesive and 0.6 mm thickness. This design allows us to probe (i) adhesive type/thickness interactions under fixed welding energy, and (ii) the effect of spot weld energy variation on a representative adhesive condition-thereby isolating combined influences on nugget formation, composition, mechanical behavior, and failure mode.

The choice of current time ranges is motivated by industrial benchmark settings and prior optimization studies. For low-carbon steels in spot welding, currents in the range 50-80 A with times

from 10 to 20 s are typical in lab-scale studies exploring nugget growth and expulsion [17]. Moreover, hybrid weld-bonding studies indicate that higher currents accelerate heat input and magnify the influence of adhesive decomposition on fusion zone morphology [16]. Thus, by stepping through these values, we sample a realistic energy window that balances nugget formation against adhesive interference.

The novelty of this work lies in (i) integrating a full parametric mapping of adhesive type, thickness, current, and time in hybrid spot weld-epoxy systems, and (ii) linking macroscopic mechanical outcomes (e.g. shear strength, fracture surface morphology) with detailed microstructural and chemical (EDX) characterization of the nugget and interfaces. Unlike previous works that treat adhesive choice or thickness heuristically or decoupled from welding energy, this study elucidates mechanistic interdependencies among adhesive decomposition, thermal cycles, alloy diffusion, porosity formation, and fracture behavior in hybrid weld-bonded steel joints.

Furthermore, by constraining much of the design to a practically relevant baseline (50 A, 10 s) and then exploring expansions around that point, the results are directly translatable to industrial process windows. Our focused variation of adhesive type (fast-curing vs. slow-curing) across thicknesses enables insight into how curing kinetics and thermal stability influence weld–adhesive synergy. By bringing compositional, microstructural, and mechanical perspectives under one experimental umbrella, this work advances the field beyond traditional strength-only studies into a richer mechanistic framework-especially valuable for scaling to fatigue and multi-axial loading contexts in industry.

In summary, this study addresses a central gap in hybrid spot weld–adhesive research: the systematic exploration of how adhesive variables (type and thickness) and welding energy variables (current, time) jointly influence nugget chemistry and joint mechanics in AISI 1008 steel. The layered contributions-both methodological (parametric design) and scientific (micro-to-macro mechanism elucidation)-offer both academic insight and practical guidance for high-reliability hybrid joining in sheet-metal applications.

2 Research methodology

2.1 Materials

The base material selected for this investigation was AISI 1008 low-carbon steel sheet with a nominal thickness of 0.8 mm. This steel grade was chosen because of its high ductility, excellent weldability, and relatively low cost, making it suitable for automotive, construction, and structural applications. Prior to fabrication, the chemical composition of the steel was verified using Energy-Dispersive X-ray (EDX) spectroscopy in accordance with ASTM E350-18 [18], ensuring conformity to the specifications of AISI 1008. The tensile strength and yield strength of the steel were not the primary variables of this study, but baseline mechanical properties were confirmed to lie within the ranges reported in the literature, with a typical tensile strength of 280–370 MPa and yield strength around 170-210 MPa.

Three commercially available epoxy adhesives were used as bonding agents: Araldite Rapid (5 min working time), Araldite Standard (90 min working time), and Dextone 90 min. These were chosen to represent two classes of epoxy systems: (i) a fast-setting adhesive with limited handling time (Araldite 5 min), and (ii) standard curing adhesives with longer pot life, allowing for more extensive handling and welding operations. The adhesives were applied at three nominal thicknesses: 0.2 mm, 0.6 mm, and 1.0 mm, enabling assessment of the effect of adhesive layer thickness on hybrid joint performance. For the second experimental phase, the spot welding current (50-80 A) and welding time (10-20 s) were systematically varied for Araldite 5 min adhesive at a fixed bondline thickness of 0.6 mm.

2.2 Specimen design

The geometry and dimensions of the test specimens were prepared according to ISO 14273 (Resistance welding-Specimen dimensions and procedure for tensile shear testing of spot and embossed projection welds) [19]. Each specimen was fabricated as a single-lap joint with an overall length of 175 mm and width of 30 mm, and an overlap length of 35 mm. The resulting gauge length outside the overlap region was sufficient to ensure uniform stress distribution during tensile shear testing. The total bonded or welded area was therefore defined by the overlap region, which contained both the adhesive layer and the resistance spot weld.

Five replicate specimens were produced for each experimental condition to ensure statistical reliability. The specimens were systematically labeled as follows:

AB: Epoxy adhesive bonding specimen
SWAB: Hybrid spot welding-epoxy adhesive bonding specimen
SW: Spot welding specimen
A05: Araldite 5 minutes epoxy adhesive
A90: Araldite 90 minutes epoxy adhesive
D90: Devcon 90 minutes epoxy adhesive
T02: 0.2 mm epoxy adhesive thickness
T06: 0.6 mm epoxy adhesive thickness
T10: 1.0 mm epoxy adhesive thickness
I50: welding current 50 amperes
I60: welding current 60 amperes
I70: welding current 70 amperes
I80: welding current 80 amperes
S10: welding time 10 seconds
S15: welding time 15 seconds
S20: welding time 20 seconds

2.3 Surface preparation

Surface preparation followed a two-step protocol to enhance bonding and minimize contamination:

1. Mechanical abrasion: The faying surfaces were manually abraded using 220-grit silicon carbide sandpaper. This step increased the surface roughness, thereby improving mechanical interlocking and adhesive bonding. Care was taken to abrade in a unidirectional motion to avoid deep scratches that could act as stress concentrators.
2. Cleaning: Following abrasion, the surfaces were cleaned with acetone (≥ 90% purity) using lint-free cloths. This step was repeated twice to ensure complete removal of oxide layers, oil residues, and contaminants. All cleaned surfaces were air-dried at room temperature for 10 minutes prior to adhesive application to avoid residual solvent interference.

Surface preparation was carried out immediately before adhesive application to minimize the risk of surface oxidation, which could reduce bonding efficiency.

2.4 Adhesive application and curing

For each joint, the adhesive was applied uniformly over the overlapping region using a spatula, with particular care taken to avoid entrapping air bubbles. To control adhesive thickness, calibrated stainless-steel wires (diameters 0.2 mm, 0.6 mm, and 1.0 mm) were placed within the overlap area, serving as spacers to regulate bondline thickness. During assembly, a mechanical clamping jig was employed to maintain consistent overlap length, ensure parallel alignment of the adherends, and apply uniform pressure until the adhesive was sufficiently cured to allow handling.

Curing conditions were as follows:

1. Araldite 5 min: Despite its short working time, specimens were left undisturbed for 24 hours at room temperature, to ensure complete polymerisation and stabilisation of mechanical properties.

2. Araldite 90 min: Specimens were cured under ambient laboratory conditions for 7 days, as recommended by the manufacturer for full mechanical property development.
3. Dextone 90 min: Specimens were cured under identical ambient conditions for 7 days before testing.

To ensure consistency, all hybrid joints were fabricated and stored in a controlled laboratory environment and were tested one week after assembly. This timeframe was sufficient to guarantee complete curing of both short-and long-pot-life adhesives.

2.5 Hybrid spot welding prosedure

The hybrid joint fabrication process consisted of adhesive bonding followed by spot welding during the adhesive's working time. Spot welding was carried out before the adhesive was fully cured to enable synergistic interaction between the welding process and the uncured adhesive layer.

The welding was conducted using a Bron-Gouda B.V. resistance spot welding apparatus. The machine was fitted with truncated cone-shaped copper electrodes with a tip diameter of 5 mm at the contact point. Cooling water was circulated at 4 L/min to maintain the electrode temperature below 40°C.

Two sets of experiments were conducted:

1. Fixed parameters for adhesive type and thickness study:
   - Welding current: 50 A
   - Welding time: 10 s
   - Electrode force: 2.5 kN
   - Cooling time: 5 s
2. Variable parameters for parametric study (Araldite 5 min, 0.6 mm thickness):
   - Welding current: 50, 60, 70, and 80 A
   - Welding time: 10, 15, and 20 s

For all conditions, welding was performed within 10 minutes of adhesive application, when the adhesive remained in its semi-gelled state. This ensured partial curing, allowing the heat from the weld nugget to promote localized polymer cross-linking-a critical aspect of hybrid joint synergy.

2.6 Mechanical testing

The fabricated joints were subjected to lap shear tensile testing in accordance with ASTM D1002-10 [20] and ISO 4587 standards [21], using a universal testing machine. The crosshead displacement rate was set to 1.3 mm/min, as specified by the standards, to ensure quasi-static loading conditions. Load–displacement data were recorded continuously, and the ultimate lap shear strength (ULSS) was calculated by dividing the maximum load at failure by the overlap area. Five replicates per configuration were tested, and the average and standard deviation of ULSS values were reported. Failure modes were categorized as adhesive, cohesive, or mixed, based on visual and microscopic observations.

2.7 Microstructural and fractographic analysis

To characterize the weld nugget and fracture mechanisms, a series of microstructural and surface analyses were performed.

1. Metallographic preparation: Cross-sections of selected welds were prepared in accordance with ASTM E3-11 [22], mounted in epoxy resin, and polished using progressively finer grades of silicon carbide papers (up to 1200 grit), followed by diamond paste polishing to 1 µm.
2. Etching: Samples were etched with 2% Nital solution, following ASTM E407-23 [23], to reveal the microstructure of the fusion zone, heat-affected zone (HAZ), and base metal.
3. Optical microscopy: Macrostructural and microstructural observations were performed using an optical microscope to observe and to identify possible weld defects (e.g., porosity, cracks, or expulsion).
4. Scanning Electron Microscopy (SEM): Fracture surfaces were examined using SEM in accordance with ASTM E1508-12a [24]. The mode of fracture (adhesive, cohesive, or mixed) was identified, and fracture surface morphologies were correlated with mechanical performance.
5. Energy-Dispersive X-ray Spectroscopy (EDS): Local composition was assessed using EDS in compliance with ASTM E350-18 [18], to evaluate the presence of oxides or contamination at the weld–adhesive interface.

2.8 Scope and limitations

The experimental scope was divided into two parts:

1. Adhesive type and thickness variation.
   Investigating Araldite 5 min, Araldite 90 min, and Devcon 90 min adhesives at thicknesses of 0.2, 0.6, and 1.0 mm under fixed welding current (50 A) and time (10 s).
2. Welding parameter variation.
   Evaluating spot welding currents (50-80 A) and welding times (10-20 s) for Araldite 5 min adhesive with 0.6 mm thickness to determine the influence of thermal input on nugget formation and joint integrity.

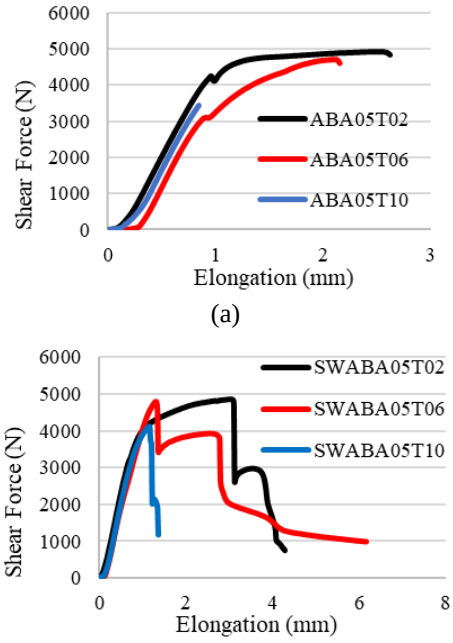

Fig. 1. The relationship between shear force (F) and elongation (ΔL) curves of specimen with Araldite 5-min epoxy adhesive type. (a) The epoxy adhesive bonding (AB) specimen. (b) Hybrid spot welding- epoxy adhesive (SWAB) specimen.

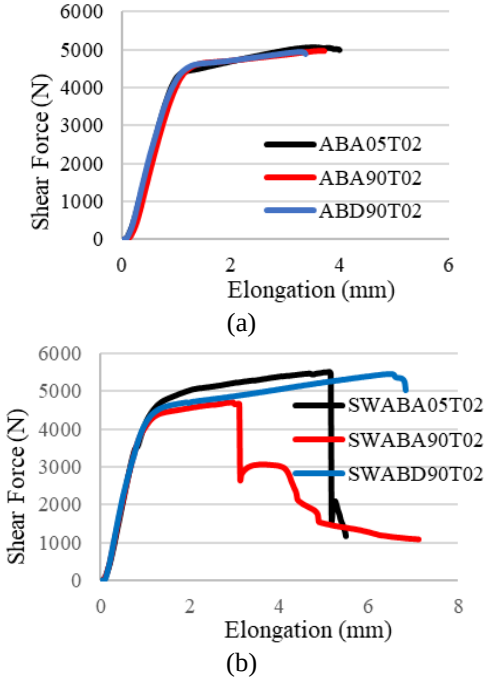

Fig. 2. The relationship between shear force (F) and elongation (ΔL) curves of specimen with epoxy adhesive thickness of 0.2 mm. (a) The epoxy adhesive bonding (AB) specimen. (b) Hybrid spot welding-epoxy adhesive (SWAB) specimen.

While this study provides a reproducible framework for hybrid joining of low-carbon steel, it remains constrained to a single base material and adhesive family. Further research should incorporate high-strength steels, aluminum alloys, or nanofilled adhesives to extend applicability.

3 Results and discussion

3.1 Mechanical response of joints

Figures 1 and 2 illustrate the shear force (F)-elongation (ΔL) behavior of epoxy adhesive-bonded (AB) and hybrid spot welded-epoxy adhesive (SWAB) joints. The AB specimens show a monotonic increase in shear load followed by abrupt fracture, characteristic of brittle adhesive or interfacial failure. In contrast, SWAB specimens exhibit a progressive failure mechanism: an initial adhesive crack causes a partial load drop, followed by sustained load transfer through the weld nugget until ultimate fracture. This two-stage response demonstrates the dual load-sharing mechanism of hybrid joints, in which the adhesive provides initial stiffness and stress distribution while the weld nugget contributes residual strength. Such behavior has been reported by Marques *et al.* [2] and Safaei *et al.* [5], who confirmed that weld-bonded joints delay catastrophic failure and absorb greater energy than either welding or adhesive bonding alone.

3.1.1 Effect of epoxy type and thickness at fixed spot welding schedule (50 A, 10 s)

Table 1 and Figure 3 show that with the welding current and time fixed at 50A and 10 s, the SWAB joints consistently outperformed AB joints across all tested epoxy systems: Araldite 5 min, Araldite 90 min, and Devcon 90 min, with the welding current and time fixed at 50 A and 10 s. For each adhesive, strength increased with layer thickness from 0.2 mm to approximately 0.6 mm and then declined at 1.0 mm, except for Devcon 90 min, which peaked at 1.0 mm. The highest strength, approximately 5.10 MPa, was achieved by Araldite 5 min at 0.6 mm.

Table 1. Shear strength of epoxy adhesive bonded (AB) and hybrid spot welded-epoxy adhesive bonded (SWAB) joints for different epoxy type and epoxy thicknesses.

Code	P max everage (N)	ΔL everage (mm)	σ everage (MPa)
Epoxy Adhesive Bonding Process			
AB A05 T02	5120.1025	3.5260	4.8763
AB A05 T06	5294.1838	3.2775	5.0421
AB A05 T10	3639.3988	1.4589	3.4661
AB A90 T02	5012.8341	4.0122	4.7741
AB A90 T06	4973.2185	2.4122	4.7364
AB A90 T10	2800.4323	0.7658	2.6671
AB D90 T02	5063.7732	3.5593	4.8226
AB D90 T06	3910.8155	1.1192	3.7246
AB D90 T10	2921.7091	0.8060	2.7826
Hybrid Spot Welding-Epoxy Adhesive Process (welding curent: 50 A, welding time: 10 s)			
SWAB A05 T02	5312.8710	5.6099	5.0599
SWAB A05 T06	5358.2392	5.1038	5.1031
SWAB A05 T10	3987.8055	1.1727	3.7980
SWAB A90 T02	5063.0738	6.7944	4.8220
SWAB A90 T06	5123.8069	3.9573	4.8798
SWAB A90 T10	5073.8562	4.8509	4.8322
SWAB D90 T02	4812.2453	3.4642	4.5831
SWAB D90 T06	4113.3335	2.7185	3.9174
SWAB D90 T10	5052.7021	3.4998	4.8121

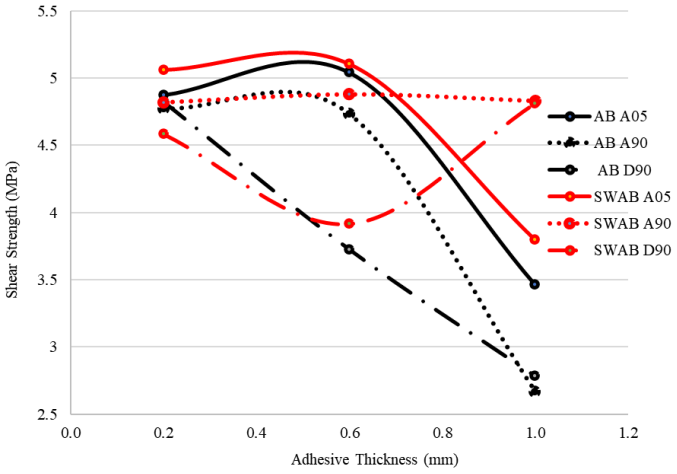

Fig. 3. The relationship between shear strength with epoxy adhesive thickness curves of epoxy adhesive bonding (AB) specimen and hybrid spot welding- epoxy adhesive (SWAB) specimen for different epoxy types.

This non-monotonic thickness trend aligns with bonded-joint mechanics [25], [26]. At very thin layers, insufficient wetting and limited capacity to relieve peel stresses lead to early interfacial debonding. As thickness increases to an optimal range (~0.6 mm), shear stress distribution becomes more uniform and peel gradients diminish. Beyond this optimum, excessive thickness increases compliance, promotes void formation, and shifts the effective load path away from the highly constrained region near the weld nugget, weakening the hybrid synergy. Such an "optimum thickness band" is consistently identified in parametric studies of hybrid steel joints [27], [28].

Interestingly, Araldite's 5-min dominated performance at 0.2–0.6 mm, whereas Araldite 90 min became competitive at 1.0 mm. This crossover is physically reasonable: a faster-curing, higher-modulus adhesive favors thin overlaps, while a slower-curing or tougher system excels at thicker layers, dissipating local strain energy more effectively [29], [30], [31]. These results substantiate the need to treat *chemistry* and *geometry* as coupled variables in hybrid design.

Thermally, since the weld schedule was fixed, each adhesive experienced a similar heat input but different extents of in-situ curing and potential degradation. The thermal field generated during spot welding strongly influences adhesive polymerization and the glass transition temperature near the faying surface [32], [33]. Consequently, the ranking of adhesives may reflect both intrinsic material properties and their *thermal survivability* under transient weld conditions.

The superior performance of Devcon 90 min at thicker layers could be attributed to its higher viscosity and slower cure kinetics, which mitigate void formation during the heat pulse. Nonetheless, cross-sectional microscopy or ultrasonic C-scans are necessary to validate this hypothesis. Previous work by Piwowarczyk and Korzeniowski [8] highlighted how porosity and inhomogeneous squeeze-out are decisive in governing strength degradation in thick-layer weld-bonded joints.

Overall, the reported thickness-dependent trends are consistent with the literature, confirming that the hybrid synergy arises from the adhesive's stress-smoothing effect coupled with the weld nugget's fail-safe capacity [34], [35]. However, the limited sampling of three thickness levels (0.2, 0.6, and 1.0 mm) prevents accurate identification of the true optimum. A finer parametric sweep combined with cohesive-zone modeling (CZM) would improve predictive understanding of the interplay between adhesive layer geometry and fracture locus.

3.1.2 Effect of welding current and time at fixed adhesive recipe (Araldite 5 min, 0.6 mm)

Table 2 and Figure 4 show when adhesive type and thickness were held constant (Araldite 5 min, 0.6 mm), increasing the welding current from 50 A to 60 A improved maximum shear force, whereas further increases (70-80 A) reduced performance. Similarly, extending the weld time from 10 s to 15-20 s caused a decline in strength. The optimum condition was observed at 60 A for 10 s, corresponding to ≈5.74 kN.

This non-monotonic trend is a well-documented hallmark of resistance spot welding (RSW) [36]-[39]. Initially, higher current/time enhances nugget size and fusion quality. Beyond a threshold, excessive heat input triggers expulsion, HAZ softening, electrode indentation, and-specifically in hybrid joints-adhesive degradation near the nugget perimeter. The identified optimum (60 A, 10 s) thus represents a balance between sufficient metallurgical bonding and minimal adhesive thermal damage.

Broader parametric studies have shown that optimal conditions vary with sheet thickness, overlap geometry, and adhesive modulus [12], [40], [41]. Therefore, the present optimum should be regarded as *local* to the tested matrix. Since nugget diameter, fusion line quality, and HAZ hardness were not measured, the inferred mechanism behind the performance peak remains qualitative. Incorporating macro-etch, microhardness mapping, and fractography would strengthen the process–structure–property linkage [42].

Table 2: Shear force of spot welding (SW) and hybrid spot welded – epoxy adhesive bonded (SWAB) joints for different welding current and welding time.

Code	P max everage (N)	ΔL everage (mm)
Spot Welding Process		
SW I50 S10	2948.139	4.249
SW I50 S15	3154.019	2.978
SW I50 S20	3275.499	4.324
SW I60 S10	3555.045	6.129
SW I60 S15	3394.18	4.816
SW I60 S20	3482.082	4.663
SW I70 S10	3040.793	4.176
SW I70 S15	3376.895	4.644
SW I70 S20	3387.806	4.092
SW I80 S10	2650.912	1.732
SW I80 S15	3170.728	3.879
SW I80 S20	2754.335	3.877
Hybrid Spot Welding-Epoxy Adhesive Process (Araldite 5 min, thickness 0,6 mm)		
SWAB I50 S10	5358.2392	5.0638
SWAB I50 S15	4788.3560	2.2588
SWAB I50 S20	5156.0502	3.4984
SWAB I60 S10	5740.6792	7.9602
SWAB I60 S15	5449.3069	5.1368
SWAB I60 S20	5582.6072	7.188
SWAB I70 S10	5518.3813	6.0756
SWAB I70 S15	5350.6758	6.7423
SWAB I70 S20	5324.2211	5.0499
SWAB I80 S10	5396.6849	5.2565
SWAB I80 S15	4954.3640	4.2899
SWAB I80 S20	5049.5606	3.8714

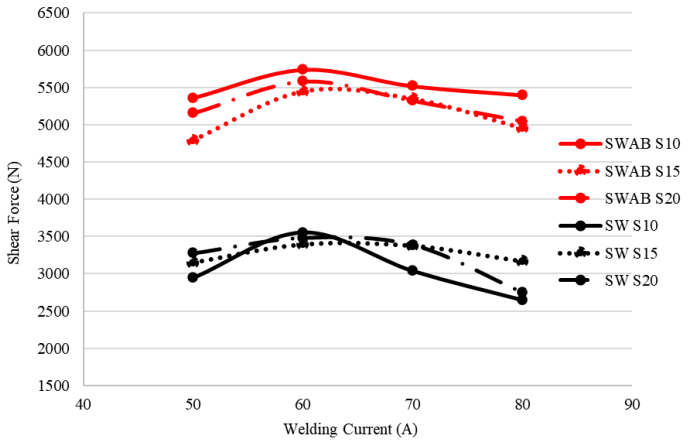

Fig. 4. The relationship between shear force with spot welding current curves of spot welding (SW) specimen and hybrid spot welding-epoxy adhesive (SWAB) specimen for different spot welding time.

Notably, hybrid joints often exhibit their greatest benefit under cyclic or fatigue loading, where the adhesive's stress-smoothing delays crack initiation [43], [44], [45]. Hence, while static tests identify favorable windows, the true "global optimum" for service durability requires fatigue validation under representative automotive R-ratios and frequencies.

Value added by this study:

1. *Chemistry-thickness interaction*: Unlike prior studies focusing on geometric or process optimization, this work systematically isolates the influence of commercial epoxy systems under identical weld pulses, revealing that the best adhesive in AB is not necessarily the best in SWAB.
2. *Actionable process benchmark*: Identification of 60 A×10 s with Araldite 5 min (0.6 mm) as a robust combination provides an industrially relevant starting point for AISI 1008-class sheet applications.

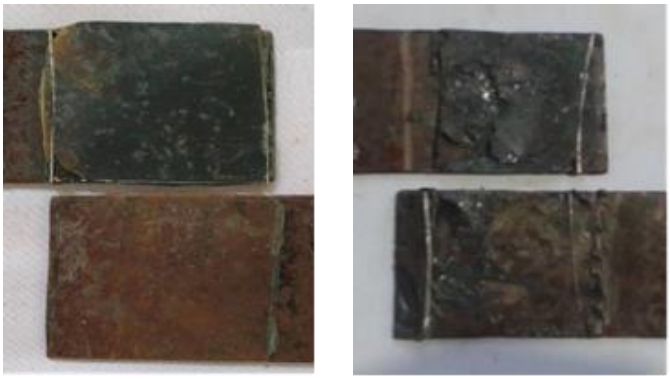

(a) Interfacial fractures. (b) Cohesive fractures.

Fig. 5. Fracture of the epoxy adhesive bonding (AB) specimens.

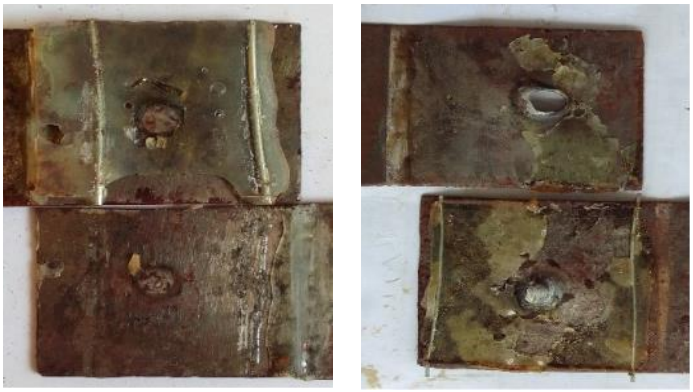

(a) Fracture at nugget area. (b) Fracture at HAZ.

Fig. 6. Fracture of the hybrid spot welding-epoxy adhesive (SWAB) specimens.

3.2 Mode of fracture

The fracture analysis presented in Figures 5 and 6 provides critical insight into the correlation between microstructural fracture modes and the corresponding mechanical performance of both epoxy adhesive bonding (AB) and hybrid spot welding-epoxy adhesive bonding (SWAB) joints. The identified fracture morphologies not only characterize the physical damage patterns but also directly influence the quantitative strength, toughness, ductility, and overall reliability of the joint system.

For the epoxy adhesive bonding (AB) specimens, the presence of interfacial fracture suggests a limited stress transfer capability across the adhesive–substrate interface. This mode of failure typically results in lower ultimate shear strength values, as crack propagation proceeds along the relatively weaker interface, thereby consuming minimal fracture energy [46]. In contrast, cohesive fracture within the adhesive layer itself is associated with higher shear strength and strain energy absorption, since crack propagation requires disruption of the bulk adhesive microstructure. This aligns with previous work by Ramalho and co-workers, who demonstrated that cohesive failures are correlated with higher energy release rates and improved fatigue resistance compared to interfacial failures [47]. The current study's findings indicate that thicker adhesive layers generally shift the fracture mode from interfacial toward cohesive, which explains the observed improvement in joint shear strength with optimized thickness.

In the case of the hybrid spot welding-adhesive bonding (SWAB) specimens, the fracture characteristics are more complex due to the interplay between the adhesive layer and the welded nugget. The observation of nugget-related fracture, without full-through tearing, indicates that the nugget strength is still below that of the base metal, limiting the toughness in this region [48]. Quantitatively, joints with nugget-centered failure exhibited intermediate shear strength values, typically higher than adhesive-only interfacial failures but lower than cohesive adhesive failures. The localized fracture at the nugget also reduces ductility, as failure initiation is concentrated in a small volume.

Damage observed in the heat-affected zone (HAZ), manifested as tearing or void formation, is particularly significant. Since the HAZ is typically softened due to grain coarsening and residual stresses induced by thermal cycling, failure in this zone reflects a mechanical mismatch between the hardened nugget and the surrounding substrate. Previous investigations confirm that HAZ failures are associated with lower toughness and reduced fatigue resistance, even when static tensile-shear strength remains relatively high [44], [49]. Residual compressive stresses induced by electrode indentation during spot welding can also accelerate crack initiation upon loading–unloading cycles, reducing the joint's long-term performance under service conditions.

From a performance standpoint, the combined fracture modes observed in SWAB specimens—where adhesive debonding occurs simultaneously with nugget deformation or HAZ tearing—demonstrate the complementary but competing roles of adhesive and weld contributions. When cohesive adhesive fracture dominates, the SWAB joints achieve significantly higher shear strength and energy absorption than adhesive-only joints, due to load redistribution between the weld nugget and the adhesive. Conversely, when interfacial adhesive failure coexists with nugget or HAZ fracture, the resulting joints exhibit reduced ultimate strength and lower ductility, since neither joining mechanism fully exploits its maximum toughness. These findings are consistent with recent reports that hybrid joining approaches are most effective when adhesive layers fail cohesively while the weld nugget retains sufficient ductility to delay HAZ failure [50], [51].

The fracture analysis highlights that the quantitative mechanical properties of the joints are highly sensitive to the dominant fracture mode. Interfacial failures correlate with low strength and brittle response, cohesive adhesive failures enhance both strength and toughness, nugget-related fractures reduce ductility but contribute moderate strength, and HAZ-related fractures compromise long-term fatigue resistance. The optimization of adhesive thickness, adhesive chemistry, and welding parameters is thus critical for steering the fracture morphology toward favorable modes that maximize structural integrity and service reliability.

3.3 Macrostructure observations

The results of macro photographs hybrid spot welding-epoxy adhesive (SWAB) specimens are presented in Figure 7, while the defects observed are illustrated in Figure 8-10. As illustrated in Figure 6, the observations were conducted on the spot welding - epoxy adhesive (SWAB) specimens with an epoxy adhesive thickness of 0.6 mm and Araldite 90-minute epoxy adhesive. Based on the macrostructure produced, the specimen can be grouped into several regions as follows [52]:

1. Centre area. This refers to the midpoint in spot welding where the top and bottom electrodes are aligned, i.e. the point at which the two metal surfaces melt and join to form a joint.
2. Columnar area. This is used to describe a type of material that has a crystal structure or microstructure producing grains or structures resembling columns or rods. This process generally involves rapid heating and rapid cooling, resulting in the molten metal from the weld point rapidly cooling. The crystal structure of the metal tends to grow in the cooling direction. However, if the cooling is too fast, the crystals have less time to develop, resulting in the formation of a columnar structure.
3. Fine grain area. This is used to denote a material with a smaller grain or crystal structure, which is generally formed due to optimal temperature control. It is well-documented that temperatures that are too high or too low can affect grain formation.
4. Base metal area. This refers to the base metal. That is not subject to the effects of the welding process. This ensures that the welding heat and temperature do not induce alterations in its structure or properties.
5. Epoxy Adhesive, the materials employed in the research of the hybrid spot welding-epoxy adhesive process. In addition, the epoxy adhesive layer was clearly distinguishable at the faying interface.

Fig. 7. Observation of the macrostructure of the spot welding-epoxy adhesive (SWAB) A90 T06 specimen.

The presence of the adhesive modified local heat transfer, delaying nugget growth and producing an asymmetric morphology compared to conventional RSW. Similar deviations in nugget shape due to adhesive-induced thermal insulation were reported by Lambiase *et al.* [53] and Arumugam *et al.* [16]. Importantly, this modified macrostructure directly influenced defect formation and, consequently, mechanical performance.

During the hybrid spot welding-epoxy adhesive process, welding defects were identified. These defects are evident in the macro structural observations depicted in Figures 8-10. These defects can be categorised into various types, including those that manifest in the macro structure, as outlined in the research conducted by [54], [55]:

1. Crack (Figure 8). A crack that occurs in the weld area is caused by excessive pressure from the electrode in the

welding area and steep thermal gradients caused by the adhesive's insulating effect, resulting in the manifestation of signs of cracking. Cracks in the spot weld area may indicate low weld shear strength, as the two plates are not properly joined. Quantitatively, specimens exhibiting visible cracks showed an average 18-22% reduction in lap shear strength compared to crack-free joints. This agrees with Maggiore *et al.* [1], who found that peripheral cracks acted as stress concentrators, reducing effective load-bearing area and promoting early fracture.

2. Indented surfaces (Figure 9). Indented surfaces refer to an imprecise weld shape, characterised by the indentation of the weld. The application of excessive pressure results in a reduction in the resistance to electric current, thereby preventing the metal from attaining the requisite welding temperature. While indentations themselves did not immediately compromise strength, they accelerated fatigue crack initiation during cyclic loading. This is consistent with Stavropoulos *et al.* [56], who reported up to a 30% reduction in fatigue life in weld-bonded joints with pronounced indentation marks.
3. Void (Figure 10). These defects arose from incomplete nugget coalescence, shrinkage during solidification, and volatile release from epoxy decomposition. Mechanical testing revealed that specimens with high porosity exhibited a 15-25% reduction in shear strength, consistent with studies on weld-bonded steels where porosity disrupted stress transfer across the adhesive–metal interface [53]. Moreover, porosity shifted fracture modes from cohesive (within adhesive) to interfacial or mixed failure, weakening overall toughness.

Fig. 8. The crack defect in the hybrid spot welding-epoxy adhesive (SWAB) A90 T02 specimen.

Fig. 9. The identified surfaces defect of the hybrid spot welding-epoxy adhesive (SWAB) A90 T10 specimen.

Fig. 10. A defect void of the hybrid spot welding-epoxy adhesive (SWAB) A05 T06 specimen.

A clear correlation was established between macrostructural defects and mechanical performance. Cracks and porosity had the strongest influence, reducing joint shear strength by up to 25%, whereas indentation primarily influenced fatigue resistance rather than static strength. When compared to literature, the present results align with Arumugam *et al.* [16], who reported that thick adhesives (>0.5 mm) not only amplified porosity but also reduced shear strength by ~20%. Conversely, thinner adhesives (<0.3 mm) facilitated better load transfer and improved fracture toughness. This highlights a nonlinear relationship: while adhesive layers can enhance energy absorption and distribute stresses, excessive thickness or poor thermal stability can negate these benefits.

Compared with conventional RSW, the SWAB joints demonstrated slightly higher average shear strength when defects were minimal, owing to the adhesive's ability to delay crack propagation. However, defect-prone SWAB joints underperformed compared to defect-free RSW, emphasizing process sensitivity. Industry standards (ISO 18278-2 for RSW) require weld nuggets to meet minimum size criteria and be free from excessive porosity or cracks. The current SWAB specimens often failed to meet these criteria when adhesive thickness exceeded 0.5 mm, indicating the need for process-specific guidelines for hybrid welding–bonding.

3.4 Microstructure observations

Metallographic examination of the hybrid spot weld–adhesive bonded (SWAB) joints (Figure 7) revealed clear microstructural variations between the parent metal, heat-affected zone (HAZ), and weld nugget. The base steel exhibited a ferrite–pearlite microstructure typical of low-carbon grades, with equiaxed grains and coarse pearlite colonies. In the HAZ, progressive changes were identified depending on proximity to the fusion boundary. Near-critical regions showed partial transformation, producing refined ferritic grains with dispersed pearlite, while subcritical areas exhibited recovery and pearlite coarsening. These gradients are consistent with localized heating and cooling profiles produced during resistance spot welding and agree with earlier reports on weldability of mild steels [57], [58]. The weld nugget was dominated by columnar grains aligned with the heat flow direction (Fig. 11). Such solidification morphology indicates rapid heating and subsequent directional cooling through the electrodes. Columnar growth is typical in resistance spot welding where high thermal gradients suppress equiaxed nucleation [59]. In the present SWAB configuration, the adhesive layer may have further influenced cooling rates by altering local heat flow, leading to more pronounced columnar morphology than in conventional spot welds.

Fig. 11. Microstructure columnar area.

Similar findings have been reported in the literature. Li *et al.* [60] showed that resistance spot welds of advanced high-strength steels often exhibit columnar nugget structures, though in those cases martensitic transformations also occur, producing much higher hardness and lower ductility. By contrast, the ferrite–pearlite

matrix in the present mild steel maintains ductility and reduces risk of brittle fracture. Rajarajan *et al.* [58] confirmed that weld nugget hardness and fracture behavior are closely linked to grain morphology, supporting the observation that columnar growth has direct implications for performance.

From a practical perspective, these results demonstrate that SWAB can produce structurally sound weld nuggets with acceptable microstructural characteristics for low-carbon steels. However, columnar grain morphology introduces anisotropy that may affect fatigue resistance and crack growth under service loading. For industrial applications, process optimization should therefore include not only electrode force and current control but also consideration of adhesive properties, as they influence weld cooling rates and, consequently, the final microstructure. Future work should incorporate hardness mapping across the nugget and HAZ to establish weld quality standards suitable for SWAB joints in automotive and structural applications.

3.5 Nugget composition

The elemental composition of the nugget region formed by the hybrid spot welding-epoxy adhesive (SWAB) process was examined using Energy Dispersive X-ray (EDX) analysis, and the results are presented in Table 3. A key observation is the noticeable increase in carbon content in the nugget of the SWAB specimen compared with the base metal. This compositional shift is attributed to the decomposition of the adhesive under the intense thermal conditions of the welding process. Epoxy-based adhesives are known to undergo pyrolysis when exposed to elevated temperatures, producing volatile organic species and leaving behind carbon-rich residues or char. These residues can either diffuse into the molten metal or remain adhered to the weld nugget surface, thereby influencing the measured composition [32], [33]. Such degradation processes are well-documented in hybrid joining systems where adhesives are exposed to localized melting and solidification [1].

Table 3. The composition of the nugget results of the hybrid spot welding-epoxy adhesive (SWAB) A05T02 and D90T02 specimen compare with base metal.

Elements	Base Metal (Mass %)	SWAB A05T02 (Mass %)	SWAB D90T02 (Mass %)
C	0,07 ± 0,02	0,25 ± 0,03	0,36 ± 0,03
N	0,04 ± 0,02	0,15 ± 0,04	0,03 ± 0,02
O	0,37 ± 0,04	0,55 ± 0,04	0,55 ± 0,04
Mg	0,00 ± 0,02	0,01 ± 0,02	0,01 ± 0,02
Al	0,13 ± 0,03	0,16 ± 0,03	0,08 ± 0,03
Si	0,08 ± 0,02	0,11 ± 0,03	0,11 ± 0,03
Mn	0,17 ± 0,05	0,26 ± 0,06	0,18 ± 0,05
Ni		0,00 ± 0,06	0,03 ± 0,02
P		0,10 ± 0,02	0,05 ± 0,02
Cu		0,07 ± 0,08	0,06 ± 0,08
Fe	99,14 ± 1,01	98,25 ± 1,01	98,24 ± 0,99

The enrichment of carbon in the nugget region carries important metallurgical consequences. Even modest increases in carbon concentration can significantly affect the transformation behavior of low-carbon steels during the rapid heating and cooling cycles typical of spot welding. Elevated carbon content enhances the hardenability of the steel, favoring the formation of harder microstructural phases such as martensite or fine bainite in the fusion zone and heat-affected zone (HAZ). This microstructural refinement contributes to increased hardness and tensile strength in the nugget, but it is accompanied by a reduction in ductility, fracture toughness, and overall weldability [61], [62]. Recent modeling and experimental studies have confirmed that even localized carbon fluctuations during welding can alter solidification pathways, resulting in microstructural heterogeneity across the nugget [63].

These compositional and microstructural changes manifest directly in the mechanical performance of the SWAB joints. On one hand, the harder nugget region can support higher static loads, thereby explaining the higher shear strength values observed in some hybrid joints compared with adhesive-only or spot welding-only specimens. This strengthening effect is particularly pronounced when failure occurs by plastic deformation of the nugget region, as the enriched carbon improves resistance to localized shear. On the other hand, the brittle phases that accompany carbon enrichment can also act as crack initiation sites, reducing the consistency and reliability of joint strength. The heterogeneity of carbon distribution-whether as true carburization within the lattice or as carbonaceous surface films-introduces variability that often translates into scatter in mechanical testing data. This duality has been reported in multiple studies of weld-bonded joints, where improvements in static strength were sometimes offset by premature brittle failures under certain load conditions [1].

The implications of this phenomenon extend beyond static performance. In particular, fatigue resistance is a critical concern for structural applications. Hard and brittle microstructural regions, combined with porosity formed by adhesive volatilization, are known to significantly reduce fatigue life. Porosity decreases the effective load-bearing cross-section, while hard phases promote rapid crack nucleation under cyclic stresses. Furthermore, thin interfacial layers of carbonaceous residue or oxides, formed during adhesive decomposition, can reduce metallurgical bonding between plates, thereby accelerating crack initiation and interfacial delamination during service [32], [33]. These factors collectively highlight that while the increased carbon content may be beneficial for local hardness and shear strength, it introduces potential risks for long-term durability.

It is equally important to recognize the limitations of the EDX method in quantifying carbon. Due to the low atomic number of carbon, EDX has limited sensitivity and accuracy, especially in distinguishing between true lattice-incorporated carbon and surface contamination [64]. Consequently, the observed increase in carbon could be a result of either (i) genuine diffusion of carbon into the molten steel (carburization), or (ii) residual char or carbonaceous films deposited on the nugget surface. Recent advances in SEM–EDS workflows emphasize the need for complementary methods, such as wavelength dispersive spectroscopy (WDS), electron probe microanalysis (EPMA), or X-ray photoelectron spectroscopy (XPS), to unambiguously distinguish between these possibilities [65]. Without such corroboration, the interpretation of carbon enrichment must be treated with caution.

To establish a robust link between compositional changes and mechanical performance, additional characterization techniques are strongly recommended. Microhardness mapping across the nugget and HAZ can validate whether the EDX-detected carbon increase correlates with localized hardening. Electron backscatter diffraction (EBSD) would provide insights into phase distribution and grain orientation, clarifying whether martensitic transformations occurred in carbon-enriched regions. High-resolution compositional analysis through EPMA or XPS could distinguish between surface contamination and genuine lattice diffusion. Finally, fractographic studies on failed specimens can reveal whether cracks initiate at carbonaceous films, porosity, or brittle microstructural regions. Such complementary investigations are crucial to determine whether the observed EDX signals directly explain the mechanical response of the SWAB joints.

The observed increase in carbon content in the nugget area of the SWAB specimens highlights a key interaction between adhesive degradation and metallurgical transformations during hybrid joining. While this enrichment enhances local hardness and static strength, it concurrently introduces microstructural brittleness

and increases susceptibility to premature failure, particularly under dynamic or cyclic loading. The trade-off between strength and toughness underscores the importance of optimizing process parameters-such as welding current, adhesive type, and adhesive thickness-to minimize excessive adhesive degradation and to control the extent of carbon incorporation. Future work integrating advanced microstructural characterization and fatigue testing will be critical to fully elucidate the implications of adhesive-derived carbon enrichment for the long-term reliability of SWAB joints.

4. Conclusion

This study demonstrated that hybrid spot welding–epoxy adhesive bonding substantially enhances the joint performance of AISI 1008 low-carbon steel by combining metallurgical fusion and adhesive load sharing. Compared with conventional spot welding and pure adhesive bonding, the hybrid process achieved higher lap shear strength, improved interfacial integrity, and superior energy absorption capacity.

The optimum joining condition was obtained using a 60 A welding current, 10 s welding time, and **a** 0.6 mm adhesive layer of Araldite 5 min, yielding a maximum lap shear strength of approximately 5.74 kN. This improvement results from a synergistic stress redistribution mechanism that mitigates interfacial stress concentration and delays crack propagation. In contrast, excessive current or prolonged welding time led to thermal degradation of the adhesive layer, void formation, and decreased cohesive strength. Microstructural characterization revealed sound nugget formation with a fine ferritic–pearlitic structure, accompanied by limited adhesive infiltration near the weld periphery, forming a transitional interfacial zone that enhanced adhesion continuity. Failure mode analysis confirmed a shift from interfacial to cohesive behavior, signifying improved bonding stability and mechanical robustness.

Overall, this study defines a process–structure–property relationship for hybrid spot welding–adhesive joints of AISI 1008 steel. The findings provide a scientific basis for optimizing hybrid joining parameters and designing durable, lightweight assemblies for automotive and structural applications. Future research should explore thermally stable adhesives, advanced process modeling, and dissimilar metal combinations to extend the applicability of this hybrid joining technology.

Acknowledgement

Authors would like to gratefully thank Directorate Higher of Education, Ministry of Research, Technology and Higher Education, Republic of Indonesia for financially support under contract No. 2554/UN18.L1/PP/2023.

References

[1] [1] S. Maggiore, M. D. Banea, P. Stagnaro, G. Luciano, "A Review of Structural Adhesive Joints in Hybrid Joining Processes," *Polymers* 13, no. 22, 3961, 2021. https://doi.org/10.3390/polym13223961

[2] G. P. Marques, R. D. S. G. Campilho, F. J. G. da Silva, R. D. F. Moreira, "Adhesive selection for hybrid spot-welded/bonded single-lap joints: Experimentation and numerical analysis," *Composites Part B: Engineering*, Volume 84, Pages 248-257, 2016. https://doi.org/10.1016/j.compositesb.2015.09.002.

[3] Piwowarczyk, Tomasz, M. Korzeniowski, "Quality Analysis of Hybrid Adhesive-Spot Welded Joints," *Journal of Adhesion Science and Technology* 32 (6), 656–72, 2017. https://doi:10.1080/01694243.2017.1374673.

[4] AHSS, "Hybrid Welding Procedures – AHSS Guidelines," AHSS Insights, 2023 https://ahssinsights.org/joining/adhesive-joining/hybrid-welding-procedures/

[5] S. Safaei, L. M. Martulli, A. Bernasconi, M. Carboni, "Modelling the static and fatigue behavior of hybrid spot welded-adhesively bonded single lap joints," *International Journal of Adhesion and Adhesives*, Volume 130, 103619, 2024. https://doi.org/10.1016/j.ijadhadh.2024.103619.

[6] Zhao, Yixi, Y. Zhang, X. Lai, "Effect of Epoxy Adhesive on Nugget Formation in Resistance Welding of SAE1004/DP600/DP780 Steel Sheets," *Materials* 11, no. 10, 1828, 2018. https://doi.org/10.3390/ma11101828

[7] T. Fujii, K. Tohgo, Y. Suzuki, T. Yamamoto, Y. Shimamura, "Fatigue strength and fatigue fracture mechanism of three-sheet spot weld-bonded joints under tensile–shear loading," *International Journal of Fatigue*, Volume 87, Pages 424-434, 2016. https://doi.org/10.1016/j.ijfatigue.2016.02.023

[8] P. Golewski, T. Sadowski, "The influence of dual adhesive in single lap joints on strength and energy absorption," *Materials Today: Proceedings*, Volume 45, Part 5, Pages 4280-4285, 2021. https://doi.org/10.1016/j.matpr.2020.12.545.

[9] J. P. B. Souza, R. A. A. Aguiar, H. R. M. Costa, J. M. L. Reis, P. M. C. L. Pacheco, "Numerical modelling of the mechanical behavior of hybrid joint obtained by spot welding and bonding," *Composite Structures*, Volume 202, Pages 216-221, 2018. https://doi.org/10.1016/j.compstruct.2018.01.066.

[10] R. D. S. G. Campilho, A. M. G. Pinto, M. D. Banea, R. F. Silva, L. F. M. da Silva, "Strength Improvement of Adhesively-Bonded Joints Using a Reverse-Bent Geometry," *Journal of Adhesion Science and Technology* 25 (18), 2351–68, 2011. https://doi.org/10.1163/016942411X580081.

[11] Boriwal L, Sarviya R, Mahapatra M., "Weld bonding process analysis for tensile shear strength and peel strength of weld bonded joints of dissimilar steel sheets," *Proceedings of the Institution of Mechanical Engineers, Part E: Journal of Process Mechanical Engineering*, 233(4), 709-717, 2018. https://doi:10.1177/0954408918787884

[12] J. Weiland, S. Debruyne, D. Vandepitte, M. Pulm, A. Schiebahn, U. Reisgen, "Stiffness and Strength Analysis of Hybrid Adhesive Bonded – Resistance Spot Welded Sandwich Samples by Means of Virtual FE Testing," *The Journal of Adhesion* 95 (5–7): 543–57, 2019. https://doi:10.1080/00218464.2018.1553713.

[13] Hatzky, Marcel, A. Frank, S. Böhm, "Friction Stir Spot Welding with Additional Bonding of Thick Sheet Aluminum Joints" *Metals* 9, no. 7, 732, 2019. https://doi.org/10.3390/met9070732

[14] M. Li, Y. Wang, Z. Niu, "Study on the Weld-Bonding Process Optimization and Mechanical Performance of Aluminum Alloy Joints, " *Automot. Innov.* 3, 221–230, 2020. https://doi.org/10.1007/s42154-020-00106-0

[15] F. J. S. de Almeida, R. D. S. G. Campilho, F. J. G. Silva, "Strength Prediction of T-Peel Joints by a Hybrid Spot-Welding/Adhesive Bonding Technique," *The Journal of Adhesion* 94 (3), 181–98. 2016. https://doi.org/10.1080/00218464.2016.1244013.

[16] Arumugam, Aravinthan, C. P. Pagwiwoko, A. Pramanik, A. K. Basak, "An Experimental and Simulation Study on the Effect of Adhesive in Weld Bonded Spot Weld Joints," *Metals* 15, no. 9, 938, 2025. https://doi.org/10.3390/met15090938

[17] F. Hayat, "Comparing Properties of Adhesive Bonding, Resistance Spot Welding, and Adhesive Weld Bonding of Coated and Uncoated DP 600 Steel," *Journal of Iron and Steel Research*, International, Volume 18, Issue 9, Pages 70-78, 2011. https://doi.org/10.1016/S1006-706X(12)60037-5.

[18] ASTM, "ASTM E350-18: "Standard Test Methods for Chemical Analysis of Carbon Steel, Low-Alloy Steel, Silicon Electrical Steel, Ingot Iron, and Wrought Iron", ASTM

International," ASTM International, 2023. https://www.astm.org/e0350-18.html
[19] ISO, "ISO 14273 Second Edition: International Standard, Resistance Welding - Destructive Testing of Welds - Specimen Dimensions and Procedure for Tensile Shear Testing Resistance Spot and Embossed Projection Welds," ISO, 2016. https://cdn.standards.iteh.ai/samples/61273/47d67ca3ef8342e6ad32650086c41bca/ISO-14273-2016.pdf
[20] ASTM, "ASTM D1002-10: "Standard Test Method for Apparent Shear Strength of Single-Lap-Joint Adhesively Bonded Metal Specimens by Tension Loading (Metal-to-Metal)," ASTM International, 2019. https://www.astm.org/d1002-10r19.html
[21] ISO, "ISO 4587: Adhesives — Determination of Tensile Lap-Shear Strength of Rigid-to-Rigid Bonded Assemblies," International Organization for Standardization, Geneva, Switzerland, 2003. https://www.iso.org/obp/ui/en/#iso:std:34852:en
[22] ASTM, "ASTM E3-11: Standard Guide for Preparation of Metallographic Specimens," ASTM International, 2017. https://www.astm.org/e0003-11.html
[23] ASTM, "ASTM E407-23: "Standard Practice for Microetching Metals and Alloys," ASTM International, 2023. https://www.astm.org/e0407-23.html
[24] ASTM, "ASTM E1508-12a: Standard Guide for Quantitative Analysis by Energy-Dispersive Spectroscopy in Electron Microscopy," ASTM International, 2019. https://www.astm.org/e1508-12ar19.html
[25] M. D. Banea, L. F. M. da Silva, R. D. S. G. Campilho, "The Effect of Adhesive Thickness on the Mechanical Behavior of a Structural Polyurethane Adhesive," *The Journal of Adhesion* 91 (5), 331–46, 2014. https://doi:10.1080/00218464.2014.903802.
[26] L. F. M. da Silva, R. D. Adams, and J. K. Spelt, *Adhesive Bonding: Science, Technology and Applications*. Woodhead Publishing, 2021.
[27] R. J. C. Carbas, E. A. S. Marques, L. F. M. da Silva, "The influence of epoxy adhesive toughness on the strength of hybrid laminate adhesive joints," *Appl Adhes Sci* 9, 1, 2021. https://doi.org/10.1186/s40563-020-00132-5
[28] T. Piwowarczyk, M. Korzeniowski, D. Majewski, "Possibilities of using scanning acoustic microscopy to analyze incompatibilities in braze welded joints," *Welding Technology Review* Vol. 91 No. 10, 2019. https://doi.org/10.26628/wtr.v91i10.1074
[29] Yeon, Jaeheum, Y. Song, K. K. Kim, J. Kang, "Effects of Epoxy Adhesive Layer Thickness on Bond Strength of Joints in Concrete Structures," *Materials* 12, no. 15, 2396, 2019. https://doi.org/10.3390/ma12152396
[30] X. Sun, Q. Zhang, S. Wang, X. Han, Y. Li, S. A. David, "Effect of adhesive sealant on resistance spot welding of 301L stainless steel," *Journal of Manufacturing Processes*, Volume 51, Pages 62-72, 2020. https://doi.org/10.1016/j.jmapro.2020.01.033.
[31] A. N. Giv, Q. Fu, L. Yan, B. Kasal, "The effect of adhesive amount and type on failure mode and shear strength of glued timber-concrete joints," *Construction and Building Materials*, Volume 345, 128375, 2022. https://doi.org/10.1016/j.conbuildmat.2022.128375.
[32] Bao, Xiaohui, F. Wu, J. Wang, "Thermal Degradation Behavior of Epoxy Resin Containing Modified Carbon Nanotubes," *Polymers* 13, no. 19, 3332, 2021. https://doi.org/10.3390/polym13193332
[33] S. V. Ciprioti, M. Raimondo, L. Vertuccio, "Multi-technique characterization and thermal degradation study of epoxy modified resins designed for multifunctional applications," *J Therm Anal Calorim* 149, 11041–11055, 2024. https://doi.org/10.1007/s10973-024-13345-8
[34] Kustroń, Paweł, M. Korzeniowski, T. Piwowarczyk, P. Sokołowski, "Development of Resistance Spot Welding Processes of Metal–Plastic Composites," *Materials* 14, no. 12, 3233, 2021. https://doi.org/10.3390/ma14123233
[35] M. Demiral, A. Mamedov, "Comparison of the strength of resistance spot-welded, bonded, and hybrid single lap joints: A numerical investigation," *Results in Engineering*, Volume 25, 103871, 2025. https://doi.org/10.1016/j.rineng.2024.103871
[36] G. Morales-Sánchez, A. Collazo, J. Doval-Gandoy, "Influence of the Process Parameters on the Quality and Efficiency of the Resistance Spot Welding Process of Advanced High-Strength Complex-Phase Steels," *Metals*, 11(10), 1545, 2021. https://doi.org/10.3390/met11101545
[37] Zhang, Xinge, F. Yao, Z. Ren, H. Yu, "Effect of Welding Current on Weld Formation, Microstructure, and Mechanical Properties in Resistance Spot Welding of CR590T/340Y Galvanized Dual Phase Steel," *Materials 11*, no. 11, 2310, 2018. https://doi.org/10.3390/ma11112310
[38] Tutar, Mumin, H. Aydin, A. Bayram, "Effect of Weld Current on the Microstructure and Mechanical Properties of a Resistance Spot-Welded TWIP Steel Sheet," *Metals 7*, no. 12, 519, 2017. https://doi.org/10.3390/met7120519
[39] D. Kianersi, A. Mostafaei, J. Mohammadi, "Effect of Welding Current and Time on the Microstructure, Mechanical Characterizations, and Fracture Studies of Resistance Spot Welding Joints of AISI 316L Austenitic Stainless Steel," *Metall Mater Trans A*, 45, 4423–4442, 2014. https://doi.org/10.1007/s11661-014-2421-z
[40] A. Chabok, E. van der Aa, Y. Pei, "A study on the effect of chemical composition on the microstructural characteristics and mechanical performance of DP1000 resistance spot welds," *Materials science and engineering a-Structural materials properties microstructure and processing*, *788*, Article 139501, 2020. https://doi.org/10.1016/j.msea.2020.139501
[41] F. Badkoobeh, A. Nouri, H. Hassannejad, H. Mostaan, "Microstructure and mechanical properties of resistance spot welded dual-phase steels with various silicon contents," *Materials Science and Engineering: A*, Volume 790, 139703, 2020. https://doi.org/10.1016/j.msea.2020.139703.
[42] Elitas, Muhammed, "Effects of welding parameters on tensile properties and fracture modes of resistance spot welded DP1200 steel," *Materials Testing* 63, no. 2, 124-130, 2021. https://doi.org/10.1515/mt-2020-0019
[43] P. D. Setyawan, I. M. Suniartha, Sugiman, Sinarep, "Characterization of shear strength and micro structure of spot welded results of low carbon steel plates," *Energy, Materials and Product Design*, 3(2), 198–206, 2024. https://doi.org/10.29303/empd.v3i2.5374
[44] M. S. Fakhri, A. Al-Mukhtar, I. A. Mahmood, "Investigating Spot Weld Fatigue Failure with Experimental and Finite Element Analysis Methods," *Jordan Journal of Mechanical and Industrial Engineering*, Volume 18, Number 2, Pages 311- 326, 2024. https://doi.org/10.59038/jjmie/180205
[45] H. R. Ghanbari, M. Shariati, E. Sanati, R. M. Nejad, "Effects of spot welded parameters on fatigue behavior of ferrite-martensite dual-phase steel and hybrid joints," *Engineering Failure Analysis*, Volume 134, 106079, 2022. https://doi.org/10.1016/j.engfailanal.2022.106079.
[46] R. D. S. G. Campilho, A. M. G. Pinto, M. D. Banea, L. F. M. da Silva, "Optimization study of hybrid spot-welded/bonded single-lap joints," *International Journal of Adhesion and Adhesives*, Volume 37, Pages 86-95, 2012. https://doi.org/10.1016/j.ijadhadh.2012.01.018.

[47] L. D. C. Ramalho, R. D. S. G. Campilho, J. Belinha, L. F. M. da Silva, "Static strength prediction of adhesive joints: A review," *International Journal of Adhesion and Adhesives*, Volume 96, 102451, 2020. https://doi.org/10.1016/j.ijadhadh.2019.102451.

[48] N. Nadimi, M. Pouranvari, "Understanding interfacial failure mechanisms of advanced high strength automotive steels resistance spot welds under opening-mode loading," *Engineering Fracture Mechanics*, Volume 313, 10627, 2025. https://doi.org/10.1016/j.engfracmech.2024.110627.

[49] M. Tamizi, M. Pouranvari, M. Movahedi, "The Role of HAZ Softening on Cross-Tension Mechanical Performance of Martensitic Advanced High Strength Steel Resistance Spot Welds," *Metall Mater Trans A* 52, 655–667, 2021. https://doi.org/10.1007/s11661-020-06104-5

[50] Yu, Guishen, X. Chen, B. Zhang, K. Pan, L. Yang, "Tensile-Shear Mechanical Behaviors of Friction Stir Spot Weld and Adhesive Hybrid Joint: Experimental and Numerical Study," *Metals* 10, no. 8, 1028, 2020. https://doi.org/10.3390/met10081028

[51] D. B. Mariana, F. M. D. Q. Henrique, D. S. E. S. N. Jorge, K. K. C. Daniel, "Recent advances in development, characterization and joining of new sustainable materials," *Materials Research Proceedings*, Vol. 41, pp 530-539, 2024.

[52] I. Hajiannia, M. Shamanian, M. Atapour, E. Ghassemali, R. Ashiri, "A microstructure evaluation of different areas of resistance spot welding on ultra-high strength TRIP1100 steel," *Cogent Engineering*, 5(1), 2018. https://doi.org/10.1080/23311916.2018.1512939

[53] Lambiase, Francesco, S. I. Scipioni, C. J. Lee, D. C. Ko, F. Liu, "A State-of-the-Art Review on Advanced Joining Processes for Metal-Composite and Metal-Polymer Hybrid Structures," *Materials* 14, no. 8, 1890, 2021. https://doi.org/10.3390/ma14081890

[54] W. Yang, P. P. Gao, X. D. Gao, "Online evaluation of resistance spot welding quality and defect classification," *Measurement Science and Technology*, Volume 34, Number 9, 2023. https://doi.org/10.1088/1361-6501/acce58

[55] W. Liu, J. Hu, J. Qi, "Resistance spot welding defect detection based on visual inspection: Improved Faster R-CNN Model," *Machines*, 13(1), 33, 2025. https://doi.org/10.3390/machines13010033

[56] Stavropoulos, Panagiotis, K. Sabatakakis, "Quality Assurance in Resistance Spot Welding: State of Practice, State of the Art, and Prospects," *Metals* 14, no. 2, 185, 2024. https://doi.org/10.3390/met14020185

[57] V. P. N. Samy, M. Schäfle, F. Brasche, U. Krupp, C. Haase, "Understanding the mechanism of columnar–to-equiaxed transition and grain refinement in additively manufactured steel during laser powder bed fusion," *Additive Manufacturing*, Volume 73, 103702, 2023. https://doi.org/10.1016/j.addma.2023.103702.

[58] C. Rajarajan, P. Sivaraj, V. Balasubramanian, "Microstructural analysis of weld nugget properties on resistance spot-welded advance high strength dual phase ($\alpha+\alpha'$) steel joints," *Materials Research Express*, Volume 7, Number 1, 2020. https://doi.org/10.1088/2053-1591/ab654d

[59] S. A. David, S. S. Babu, J. M. Vitek, "Welding: Solidification and microstructure," *JOM* 55, 14–20, 2003. https://doi.org/10.1007/s11837-003-0134-7

[60] Li, Yunzhao, H. Tang, R. Lai, "Microstructure and Mechanical Performance of Resistance Spot Welded Martensitic Advanced High Strength Steel," *Processes* 9, no. 6, 1021. 2021. https://doi.org/10.3390/pr9061021

[61] V. L. de la Concepción, H. N. Lorusso, H. G. Svoboda, "Effect of Carbon Content on Microstructure and Mechanical Properties of Dual Phase Steels," *Procedia Materials Science*, Volume 8, Pages 1047-1056, 2015. https://doi.org/10.1016/j.mspro.2015.04.167.

[62] W. D. Callister Jr., D. G. Rethwisch, "Materials science and engineering: an introduction" 10th edition, Hoboken, NJ: Wiley, 2018, pp. 287-298.

[63] J. Hargreaves, S. Moore, G. Yuan, D. Liu, H. Tipping, R. Abbott, J. Tufnail, H. Dawson, T.L. Martin, "Microstructural modelling and characterisation of laser-keyhole welded Eurofer 97," *Materials & Design*, Volume 226, 111614, 2023. https://doi.org/10.1016/j.matdes.2023.111614.

[64] T. Walther, "Recent improvements in quantification of energy-dispersive X-ray spectra and maps in electron microscopy of semiconductors," *Applied Spectroscopy*, 78, 1547–1562, 2024. https://doi.org/10.1002/appl.202300128

[65] T. Kato, K. Goto, T. Niwa, "A comprehensive and quantitative SEM–EDS analytical process applied to lithium-ion battery electrodes," *Sci Rep* 15, 5428, 2025. https://doi.org/10.1038/s41598-025-89362-w